frontiers in Marine Science

ORIGINAL RESEARCH
published: 29 September 2021
doi: 10.3389/fmars.2021.722599

Atypical Diagenesis and Geochemistry of Redox-Sensitive Elements in Hydrothermal Sediments of the Southern Okinawa Trough

Li Li[1,2], Duc Huy Dang[3], Xiaojing Wang[1], Jihua Liu[1,2], Yonghua Wu[1], Aimei Zhu[1,2] and Xuefa Shi[1]*

[1] Key Laboratory of Marine Geology and Metallogeny, First Institute of Oceanography, Ministry of Natural Resources, Qingdao, China, [2] Laboratory for Marine Geology, Qingdao National Laboratory for Marine Science and Technology, Qingdao, China, [3] Trent School of the Environment and Chemistry Department, Trent University, Peterborough, ON, Canada

Early diagenesis processes and the geochemistry of redox-sensitive elements (RSEs) in four sediment cores in an active hydrothermal field in the southern Okinawa Trough (OT) was investigated. Dissolved Fe, Mn, ΣHS^-, and several other RSEs (Mo, U, and V) in pore water were measured. We also studied metal distribution in sediments using sequential extraction methods. Very high dissolved Fe concentrations (~140 μmol L^{-1}) but insignificant dissolved Mn were observed in surficial pore waters in the station adjacent to the hydrothermal vent, where highly reactive Fe, Mo, U in the sediments were also measured. Such an atypical diagenetic sequence found in those cores could be driven by the overwhelmingly high reactive Fe fraction (mostly Fe oxides) delivered from the vents. Consequently, significant upward benthic fluxes of Fe and Mo were estimated for the studied stations. In addition, we performed a principal component analysis (PCA), together with relative ratios of carbonate-related elements (Sr, Ca, Mg), to identify particles' origins in the hydrothermal field; two endmembers being the hydrothermal source and hydrogenous processes. This comprehensive study on a unique set of samples collected by advanced technology provided valuable data to demonstrate distinctive geochemical features that occur in hydrothermal sediments.

Keywords: hydrothermal, early diagenesis, benthic flux, iron, redox-sensitive elements, Okinawa Trough

OPEN ACCESS

Edited by:
Aaron J. Beck, GEOMAR Helmholtz Center for Ocean Research Kiel, Germany

Reviewed by:
Zhilei Sun, Qingdao Institute of Marine Geology (QIMG), China
Tomoko Komada, San Francisco State University, United States

****Correspondence:***
Li Li
Li.Li@fio.org.cn

Specialty section:
This article was submitted to Marine Biogeochemistry, a section of the journal Frontiers in Marine Science

Received: *09 June 2021*
Accepted: *16 August 2021*
Published: *29 September 2021*

Citation:
Li L, Dang DH, Wang X, Liu J, Wu Y, Zhu A and Shi X (2021) Atypical Diagenesis and Geochemistry of Redox-Sensitive Elements in Hydrothermal Sediments of the Southern Okinawa Trough. Front. Mar. Sci. 8:722599. doi: 10.3389/fmars.2021.722599

INTRODUCTION

Submarine hydrothermal vents are a widespread feature of the ocean seafloor, not only in the mid-ocean ridges, but also in the island arcs (Hawkes et al., 2014; Beaulieu et al., 2015). Since their first discovery in late 1970s, hydrothermal vents are recognized as a potentially important source and sink of elements in the deep ocean (Edmond et al., 1979). Once discharged by the hydrothermal fluids into the cold and oxygenated seawater, the dissolved metals were believed to mostly precipitate as sulfides or oxides and scavenged out of the water column to sediments surrounding the vents (Elderfield and Schultz, 1996). The hydrothermal/volcanic influenced sediments are typically fine-grained, rich in metals and have high surface area/weight ratio; therefore, they are prone to biogenic activities, and early diagenetic processes may play an important role governing

the biogeochemical cycles of trace metals in those sediments (Homoky et al., 2011). However, by far, studies reporting the early digenesis processes of metals in hydrothermal/volcanogenic sediments are scarce.

Homoky et al. (2011) have studied the diagenesis of Fe and Mn in volcanogenic sediments and estimated significant upward benthic fluxes of colloidal Fe and Mn based on pore water and overlying water concentrations. Aquilina et al. (2014) studied sediments from a submarine volcanic edifice in the Bransfield Strait, Antarctica. Dissolved Fe concentrations in surface pore water were also low (< 2 μM) due to an oxic sediment layer overlaying the subsurface peak (565 μm). However, the authors suspected that, through a breach of the surface oxic layer related to the abundant benthos (i.e., tubeworm), the sediments may be an important source of Fe and Mn to the deep waters. On the other hand, the geochemistry of other redox-sensitive elements (RSEs) in hydrothermal sediments is expected to be significantly distinct from other deep-sea oxic sediments because geochemical cycling processes of RSEs are greatly affected by redox changes and the reactive surfaces of newly formed materials in the hydrothermal environment. Overall, our understanding of how early diagenesis processes affecting those metals' geochemistry in hydrothermal sediments remains largely fragmented. This is likely due to the difficulties in finding steadily deposited sediment layers close to the hydrothermal vents and collecting such sedimentary materials near the vents.

The Okinawa Trough (OT) is a region of great interest to conduct such investigations. The Trough is a heavily sedimented back-arc basin behind the Ryukyu Arc in the western Pacific, off the coast of Japan (**Figure 1A**). Over the past 30 years, submarine hydrothermal activities have been constantly reported in the area, especially in the middle and southern OT (Chen et al., 1995; Glasby and Notsu, 2003). Here, we reported data from four short sediment cores in near-field hydrothermal sediments in the southern OT, which were collected using a remotely operated vehicle (ROV) equipped with a robotic arm. Pore water samples were carefully retrieved and analzyed for diagenetic tracers (Fe, Mn, ΣHS^-) and several RSEs (e.g., Mo, U, V), along with their bulk concentrations in sediments. Sequential leaching experiments were also conducted on those sediments to assess the metal distribution in sediments. Atypical diagenesis processes were found in those hydrothermally influenced sediments. This study thus provides valuable data to shed light on the diagenetic processes and geochemistry of those metals in near-field hydrothermal sediments.

THE STUDY AREA

The OT spans over 1,200 km in length, is 60–100 km wide in the southern OT, and reaches a maximum width of 230 km in the northern end. Overall, the OT spans over a total area of approximately 1.5×10^5 km^2. The water depth is greatest in the southern OT (ca. 2,300 m) and gradually decreases to ca. 200 m in the northern OT (Sibuet et al., 1987; **Figure 1A**). The seafloor of the OT is covered with thick terrigenous muddy sediments; their depths increase from ∼3 km in the southern OT, to ca. 5 km in the middle OT, and up to 8 km in the northern end (Sibuet et al., 1987; Suzuki et al., 2008; Tsuji et al., 2012). These sediments originate from Eurasia, mainly from the Yangtze and Yellow Rivers, or Taiwan (Narita et al., 1990; Honda et al., 2000; Dou et al., 2010).

The subduction of the Philippine Sea Plate beneath the Eurasian Plate formed the OT; tectonic processes likely initiated and sustained hydrothermal activities observed in the middle and southern OT (Glasby and Notsu, 2003). The first visual observations of hydrothermal activities in the OT and the back-arc environment dated back to the 1980s (Halbach et al., 1989; Zhai et al., 2001). Since then, more hydrothermal fields were discovered across the OT (Watanabe et al., 2006; Kawagucci et al., 2011); exceptionally high heat flow was observed in the middle and southern OT (Yamano et al., 1989; Kinoshita et al., 1990). Black and white hydrothermal smoker vents emit hot fluids with temperatures up to 330°C (Inagaki et al., 2006). Cold-seep carbonates, bubbles from gas hydrates from sediment cores, emission of cold liquid CO_2, and shallow hydrothermal vents were also found in the southern OT (Kuo and Chen, 2000; Machiyama et al., 2001; Konno et al., 2006).

The Kuroshio Current, one of the major currents along the western boundary of the northwestern Pacific, originates from subtropical regions and enters into the OT's southwest through the deep sill in the northeast of Taiwan. The Current turns east following the bottom topography, goes northeastward along the shelf break, flows out through the Tokara Strait of Japan, and finally enters the NW Pacific Ocean (**Figure 1B**; Kao et al., 2006; Matsuno et al., 2009). The two areas identified with high-temperature venting activities in the southern OT are Hatoma Knoll (HK, 24°51.3′ N, 123°50.5′ E, depth = 1,457 m) and Yonaguni Knoll IV (YK, 24°50.9′N, 122°42.0′E, depth = 1,408 m) (**Figure 1B**). The vicinity area of the latter is also referred to as the Southernmost Part of Okinawa Trough (SPOT) area (Glasby and Notsu, 2003). Our sampling sites are located within the SPOT area where seven active venting sites and several dead chimneys have been identified (Gena et al., 2005).

MATERIALS AND METHODS

Sample Collection

In June 2016, four sediment cores (ROV 10-1, ROV 10-2, ROV 11-1 and ROV 11-2) were collected in the SPOT area (**Figure 1**), from the *R/V Ke Xue* using the *ROV Fa Xian*. These cores were retrieved by pushing the core tubes (9.5 cm inner diameter) into the sediments with the robotic arm of the ROV. The water depths of the stations were between 1,165 and 1,327 m. Core ROV10-1 was collected in a place very close to a small hydrothermal vent (**Figure 1C**), with a diameter of ca. 30 cm.

Immediately after retrieving the cores, pore water was collected using a Rhizon sampler (Rhizonsphere Inc., Netherlands) inside N_2-filled glove bags. We coupled the Rhizon sampler with thin Teflon lines and a peristaltic pump (LongerPump® Inc., China), which formed a trace-metal clean sampling pathway for pore water samples. On the *R/V Ke Xue*, pore water samples were collected in 1-cm intervals in the top

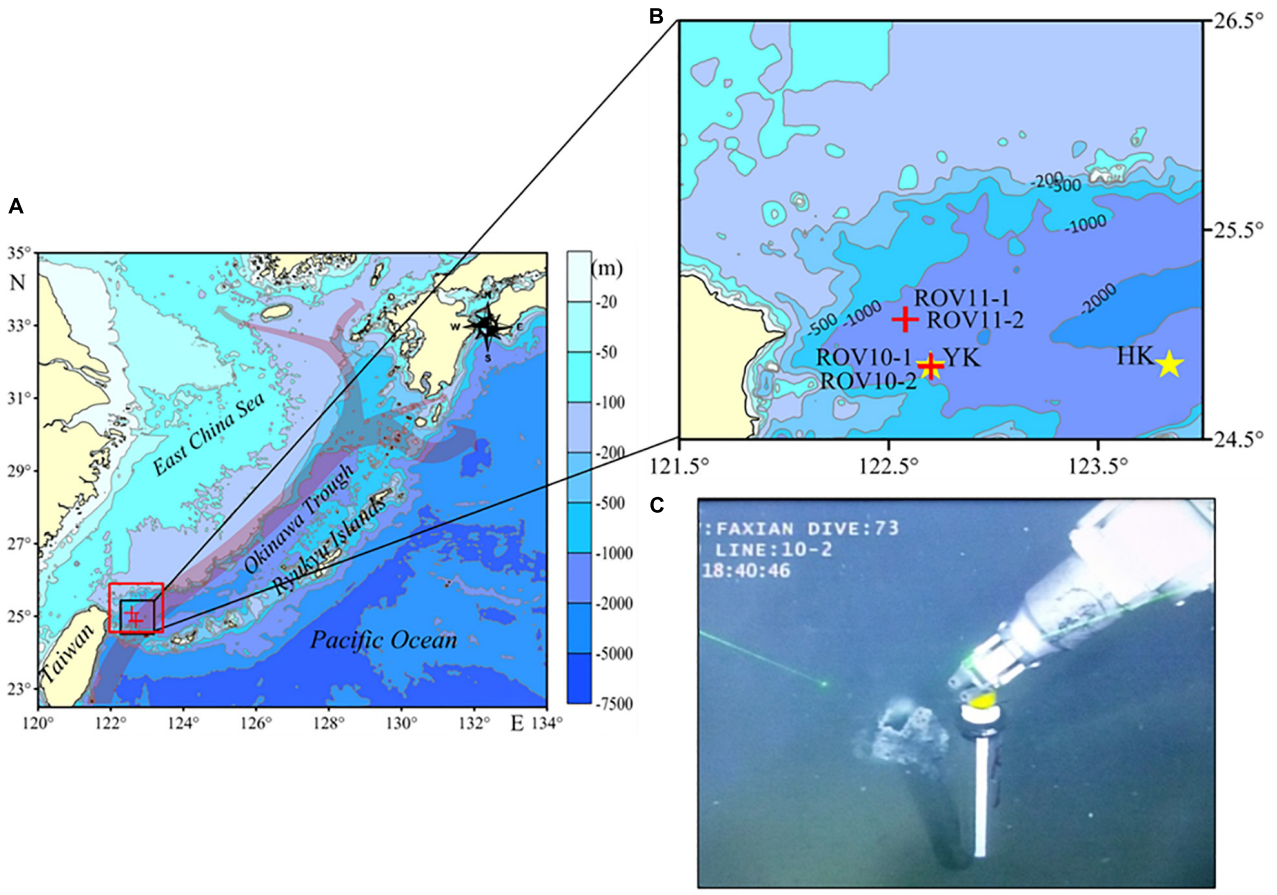

FIGURE 1 | (A) Locations of the sampling sites in the southern Okinawa Trough: gray arrows indicates the flow path of the Kuroshio Current (redrawn from Kao et al., 2006), the red rectangle indicates the location of SPOT (adapted from Glasby and Notsu, 2003). **(B)** Expanded view of the sampling locations: red crosses indicate the sampling locations, and yellow stars indicate the locations of Yonaguni Knoll (YK) and Hatoma Knoll (HK). **(C)** Picture of core ROV10-1 being collected by the robotic arm of the ROV.

10 cm and every 2 cm downcore, placed into 15 mL BD Falcon tubes, then acidified to pH∼2 with HNO_3 (Optima® grade, Thermo Fisher Scientific Inc.). The samples were stored at 4°C until analysis. Once pore waters were extracted, we sectioned the sediment cores at 1-cm intervals.

Bottom seawater samples (∼50–100 m above the seafloor) were collected using a Niskin water sampler mounted on the CTD-rosette. Seawater samples were brought to the surface and filtered immediately through 0.2 μm AcroPak® filters (Pall Inc.) into LDPE bottles (Nalgene™, Thermo Fisher Scientific Inc.), and acidified to pH ∼2 with HNO_3. The filters, tubes, sampling bottles, and any other labware that had been in contact with the samples were thoroughly cleaned, following cleaning procedures used for trace metals (details in Li et al., 2015).

Sample Analysis

Total dissolved sulfide (ΣHS^-) was measured on board the *R/V Ke Xue* with a spectrophotometer (7,200 series, Shanghai Unico Inc., China) that was placed inside a N_2-filled glove bag, using the methylene-blue colorimetric method (Cline, 1969) with a detection limit of 1.8 μmol L^{-1}. Pore water and bottom seawater samples were diluted 20-fold with 2% HNO_3 for metal analysis. Iron and Mn in pore water were analyzed using ICP-OES (6,300, Thermo Fisher Scientific Inc.), whereas Mo, U, and V in seawater and pore water were measured by collision cell ICP-MS (Thermo X Series 2, Thermo Fisher Scientific Inc.). Indium was added to all samples as an internal standard to a final concentration of 10 ppb. Analytical recoveries of Mo, U, and V analysis were determined using NASS-6 certified reference material (National Research Council, Canada). Measured values were in good agreement with the certified values (**Supplementary Table 1**). Because Mn and Fe concentrations were much higher in pore water than in the reference seawater, precision and accuracy were determined using the standard addition method. Ten percent of the samples were randomly selected and spiked with Fe and Mn standards (High-Purity Standards, United States) to two incremental concentrations to correct for any matrix effects.

Sediment samples (∼50 mg) were freeze-dried and digested with a concentrated acid mixture (HNO_3/HF, 1/1). Major elements (e.g., Al, Fe, Mn, P, Ti, etc.) were analyzed by ICP-OES and trace elements (e.g., Mo, U, V, Cd, Co, etc.) by ICP-MS. See **Supplementary Table 2** for the full list of all the elements

analyzed. A series of sediment reference standards from China (GBW07309) and Canada (MESS-3 and PACS-2) was processed to assess the accuracy of the methods. Recoveries of all elements were within the range of 92–109% (n = *15*). Total organic carbon (TOC) was determined with an Elemental Analyzer (Model EL-III, Vario); acetanilide (GBW060239) was used to assess analytical recovery (96–104%, n = 12). Relative errors observed on triplicate analyses were less than 6%. Grain sizes were determined using a laser particle size analyzer (Master Sizer 2,000, Malvern Instrument) and categorized as clay (<4 μm), silt (4–63 μm), and sand (>63 μm).

Selected sediment samples from cores ROV10-1 and ROV10-2 were subject to sequential extraction to assess metal distribution in the sediments. Iron speciation was determined using the method developed by Poulton and Canfield (2005). Sequentially extracted fractions of Fe included Fe_{CAE} (carbonates, adsorbed, or exchangeable), iron crystalline oxides, Fe_{OX} (e.g., goethite and hematite), Fe_{MAG} (magnetite) and Fe_{PY} (pyrite). The Fe_{CAE} fraction was extracted with Na acetate (pH 4.5, 48 h, 50°C). Fe_{OX} was extracted with dithionite (pH 4.8, 2 h, room temperature). Fe_{MAG} was extracted with oxalate (pH 3.2, 6 h, room temperature). Finally, Fe_{PY} (pyrite) was quantified using chromous chloride extraction (Burton et al., 2008). The sum of Fe_{CAE}, Fe_{OX}, Fe_{MAG}, and Fe_{PY} was assumed to be highly reactive iron (Fe_{HR}). Therefore, the residual refractory Fe pool was calculated as the difference between Fe_{HR} and the total Fe. The distribution of Mo, U and V in sediments was based on the modified BCR method, which partitions the elements into four fractions including acid-soluble, reducible, oxidizable and residual (Rauret et al., 1999). Further details are provided in the supporting information **Supplementary Text 1**.

Multivariate Statistical Analysis

We applied a principal component analysis (PCA) using a Matlab algorithm to examine correlations between elements and similarities among samples (see Dang et al., 2015 for further details).

RESULTS

Vertical Profiles in Pore Water

The vertical profiles of dissolved Fe, Mn, Mo, U, V and ΣHS^- in pore water of the four stations are shown in **Figure 2**. Iron and Mn profiles in ROV 10-1 revealed distinct geochemical features to other deep-sea oxic sediments (**Figure 2A**). High Fe concentrations (∼138 μM) were found in surficial (0–7 cm) pore water in ROV 10-1, then decreased sharply in deeper sediments. In contrast, dissolved Mn concentrations remained relatively low (8.5 ± 0.5 μM, n = *9*) in the surface layers of ROV 10-1 before it increased to 29.5 μM at the bottom of the sediment core. The profile of ΣHS^- was similar to that of Mn (**Figure 2A**). At station ROV 10-2, there was a subsurface peak at 3 cm in both Mn and Fe profiles (26.7 and 78.9 μM, respectively), which decreased sharply to 4.0 ± 0.5 μM and 1.8 ± 0.8 μM, respectively (n = 10) downcore (**Figure 2C**). On the other hand, ΣHS^- concentrations remained low in the top 7 cm (<100 μM) then increased steadily with depth, reaching ∼2.4 mM downcore. Based on the field observation, yellowish elemental sulfur was visible in ROV 10-2 sediments, which may support the relatively high ΣHS^- concentrations of this core.

No dissolved sulfide was detected in the pore water of core ROV11-1 and 11-2. In contrast, relatively high dissolved Fe concentrations (∼50–60 μM) were also measured in surficial (<2 cm) pore water in ROV11-2, which then decreased to zero at depth ∼15 cm. A similar vertical profile was observed for Mn with a much lower concentration (5.5 μM) in surface pore water. In core ROV11-1, deficient concentrations of dissolved Fe and Mn (<5 μM) were found in surficial sediment pore water (<2.5 cm). In deeper sediments, Mn and Fe concentrations peaked at 4.5 and 9.5 cm, respectively. This core was the shortest (i.e., 14 cm) of the four sediment cores; dissolved Mn and Fe concentrations remained high (ca. 50 and 170 μM, respectively) in pore water till the bottom of the core.

In general, dissolved concentration profiles of Mo, U, and V assessed in this study were similar among the cores; we observed a decreasing trend downcore observed at all four stations (**Figure 2**). Molybdenum and V profiles were both significantly correlated to U (r^2 = 0.43 and 0.45; n = 70, respectively, $p < 0.01$). There were subsurface peaks of all three RSEs at 2, 5.5 and 15 cm in ROV 10-1, 10-2, and 11-2, respectively. Also, because sulfide increased significantly with depth in ROV 10-2 (**Figure 2C**), Mo dropped to < 5 μM whereas U and V were not removed from pore water (**Figure 2D**).

Sediment Geochemistry

Bulk Metal Concentrations in Sediment and PCA Analysis

The sediments collected from the southern Trough were categorized as fine-grained; the grain size distribution generally varied within the classes of sandy silt, clayey silt, and silt (**Supplementary Figure 1**). The average TOC concentrations for ROV10-1, ROV10-2, ROV11-1 and ROV11-2 were 0.68 ± 0.10, 0.65 ± 0.03, 0.72 ± 0.09% and 0.78 ± 0.04%, respectively, with little vertical variation (**Supplementary Figure 2**).

Vertical distributions of a few representative major elements (Al, Mg, Fe, Mn) and three RSEs are shown in **Figures 3**, **4**, respectively. Iron was enriched (up to 7%) in the top sediments of ROV 10-1, while its concentrations remained constant with depth (4.2 ± 0.2%, n = 52) in all three other cores (ROV 10-2, 11-1 and 11-2). The highest Mo and U concentrations (up to 28 and 12 μg g^{-1}, respectively) were observed in sediments from ROV 10-1, with Mo being enriched in the top 5 cm and U enriched in the middle of the core (∼12 cm) (**Figure 4**).

We performed a PCA, based on a dataset that included 29 elements in 70 sediment samples. Two principal components (PCs) explained 62% of the variations within the dataset (**Figure 5**). Within the 29 elements assessed, three major groups were identified (**Figure 5A**): the first one comprised of a series of lithogenic elements (e.g., Li, Al, Ti), the second group included carbonate-related elements (e.g., Mg, Ca, and Sr), and the third group consisted of trace metals (e.g., Cu, Cd, Mo, U, Zn). In addition, this multivariate approach allowed the separation of

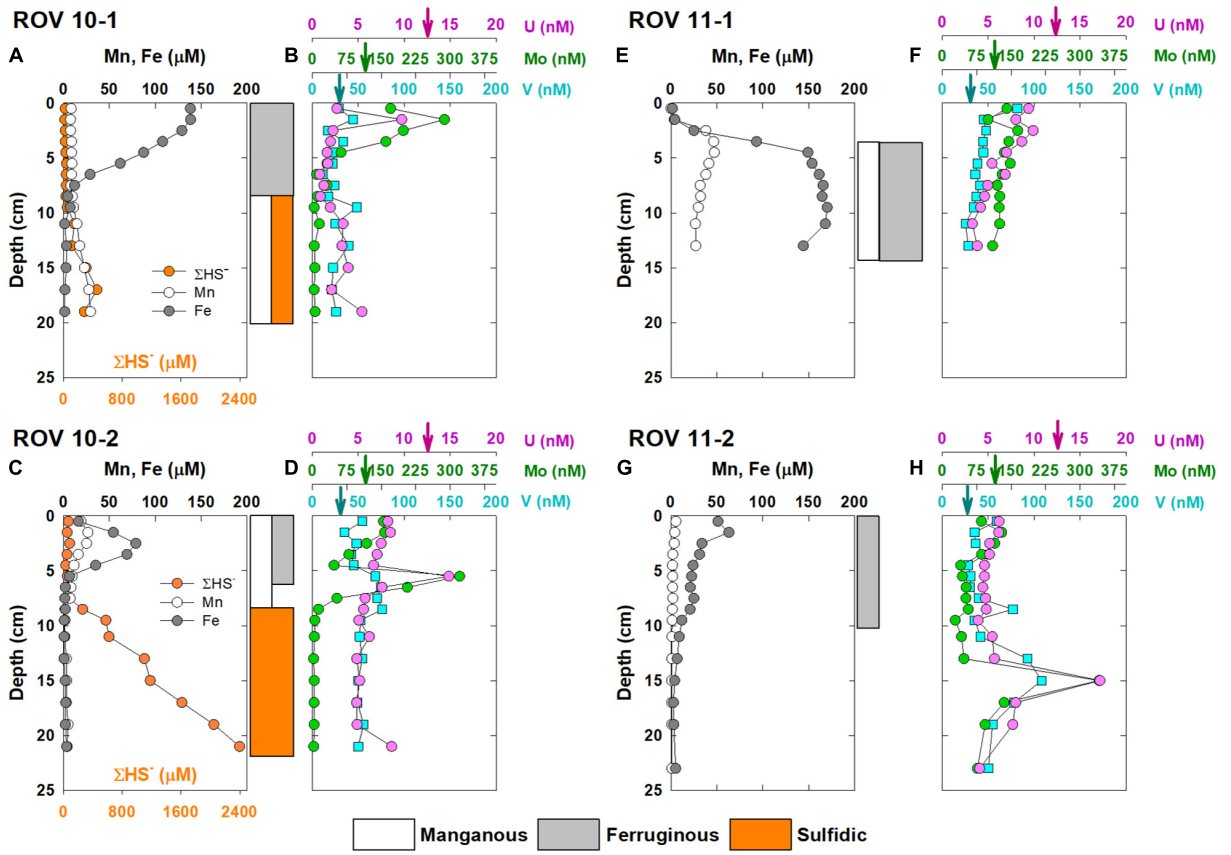

FIGURE 2 | Vertical concentration profiles of dissolved Fe, Mn, ΣHS^-, Mo, U and V in core ROV 10-1 **(A,B)**, ROV 10-2 **(C,D)**, ROV 11-1 **(E,F)**, and ROV 11-2 **(G,H)**, collected from the southern Okinawa Trough. The arrows indicate concentrations of RSEs (Mo, U, V) in the overlying water column. The color-coded blocks on the right of the figures demark the dominant diagenetic reactions (e.g., manganous, ferruginous, and sulfidic) in corresponding layers of sediments.

the four sediment cores into three groups (**Figure 5B**), ROV 10-1, which was the station adjacent to the hydrothermal vent (**Figure 1C**), ROV 11-1 and ROV 10-2/ROV 11-2.

Aluminum (**Figures 3A,B**) is representative of the first group of elements, which included those of lithogenic origin (e.g., Al, Li, K, Ti) and a few trace elements (Cr, V, **Figures 4E,F**). They show a small variation in concentrations in all four sediment cores ([Al] = 8.3 ± 0.4%, *n* = *70*). However, a slight Al enrichment could be observed in deep sediments (~ 9%) compared to surface sediments (~ 8%) in both the ROV 10-1 and 10-2 stations (**Figure 3A**). In the other two stations (ROV 11-1 and 11-2), Al concentrations were almost constant throughout the core, 8.1 ± 0.1%, and 8.3 ± 0.2%, respectively (**Figure 3B**).

The second group involved the marine carbonate elements, i.e., Ca, Mg, and Sr; their profiles were constant at station ROV 10-1 ([Mg] = 1.27 ± 0.05%, *n* = 18) and ROV 11-1 (1.60 ± 0.02%, *n* = 19) (**Figures 3C,D**). At stations 10-2 and 11-2, Mg profiles were constant in deep sediments (below 10 cm, ~ 1.4%) but showed enrichment in the top surface sediments (~ 1.6%, **Figures 3C,D**). The third group of elements included trace elements represented by Mo and U, having a large variability in their concentrations. Sediments from ROV 10-2 and 11-2 had similar and typical increasing Mo and U concentrations with depth (**Figures 4A,B**); this profile has been often observed in suboxic sediment environments (Shaw et al., 1990; Morford and Emerson, 1999). However, very high Mo and U concentrations ([U] and [Mo] up to 12 and 28 μg g^{-1}, respectively) were measured in sediments from ROV 10-1 with Mo enrichment observed just below the sediment-water interface (SWI) (**Figure 4A**). On the other hand, at ROV 11-1 neither Mo nor U was significantly enriched in the sediments ([Mo] = 0.5 ± 0.1 μg g^{-1} and [U] = 2.4 ± 0.3 μg g^{-1}, *n* = 19).

Several other elements did not significantly correlate (e.g., Fe, Ni, Th, **Figure 5A**). As mentioned above, Fe profiles in ROV 10-1 were significantly different from three others, which was expected because of its location close to the hydrothermal vent (**Figure 1**). Lastly, there was a significant correlation between Mn and P ($r = 0.68$, $p < 0.001$, $n = 70$, **Supplementary Table 3**), thus only Mn profiles are shown in **Figure 3**. These two elements have similar concentrations in deep sediments with an enrichment in the top surface sediments (**Figures 3G,H**). An enrichment factor was calculated as the ratio of total Mn concentrations just below the SWI to the average concentration in deep sediments. Accumulation of these elements decreased in order of ROV 10-2 > 11-1 > 11-2 > 10-1 and the enrichment factors were 3.4, 2.9, 1.9, and 1.2, respectively.

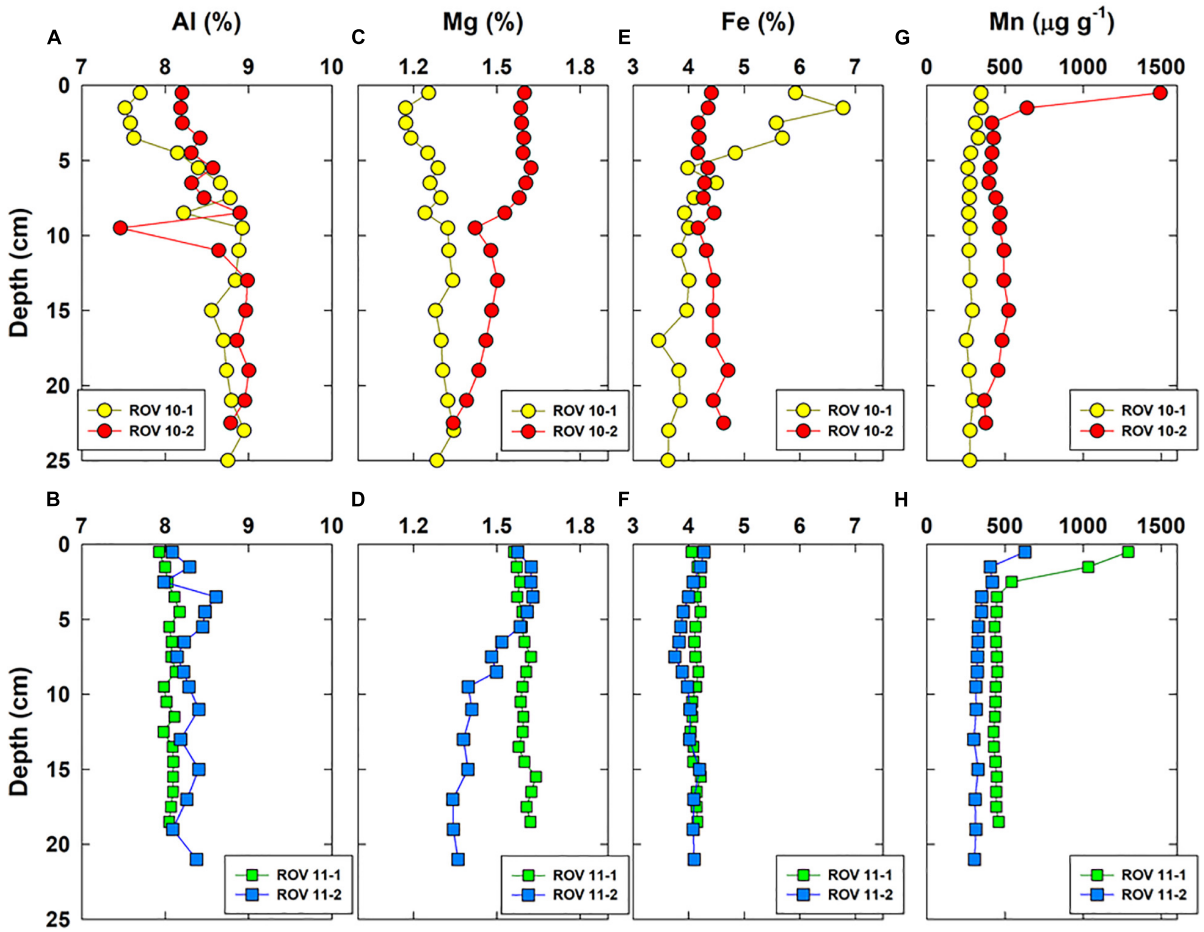

FIGURE 3 | Vertical concentration profiles of Al **(A,B)**, Mg **(C,D)**, Fe **(E,F)**, and Mn **(G,H)** in bulk sediments of the four cores collected from the southern Okinawa Trough.

Metal Distribution in Sediments

Sequential extraction of metals in cores ROV10-1 and ROV10-2 is shown in **Figure 6**. The percentages of Fe_{HR}, which includes Fe_{OX}, Fe_{CAE}, Fe_{MAG}, and Fe_{Py}, were more significant in surface layers (31–42%) relative to deeper sediments (8.5–20%). This range was similar to the distributions of Fe_{HR} in coastal sediments (Raiswell and Canfield, 2012). The Fe_{HR} enriched in the surface layers of ROV 10-1 (∼30%) were almost threefold higher than those in the bottom layer (∼10%). Total Fe concentrations (5.6–6.8%) in ROV 10-1 were also higher than the three other cores (**Figure 3**). Among the reactive Fe fractions, there was a transition between Fe_{OX} and Fe_{MAG} at ROV 10-1; Fe_{OX} represented ∼42–57% of Fe_{HR} in the top 5 cm, while Fe_{MAG} dominated below 5 cm (38–61% of the Fe_{HR}). However, no clear trend was observed for Fe_{OX} and Fe_{MAG} in ROV 10-2. Fe_{CAE} represented 23 ± 7% and 35 ± 7% of Fe_{HR} in ROV10-1 and 10-2, respectively. Finally, Fe_{PY} increased with depth in both cores; up to 16 and 4% of total Fe_{HR} in ROV10-1 and ROV 10-2, respectively.

Molybdenum distributions in the sediments were significantly different between the two sediment cores as were total Mo concentration (**Figures 4A**, **6**). In ROV 10-1, very high concentrations of Mo were measured in both residual (14.6 ± 4.9 μg g^{-1}, $n = 12$) and reactive (4.9 ± 2.4 μg g^{-1}, $n = 12$) fractions. However, both residual and reactive Mo concentrations were significantly lower at ROV 10-2 (4.4 ± 2.3 μg g^{-1} and 0.7 ± 0.4 μg g^{-1}, respectively, $n = 11$). Similarly, higher reactive U was observed in ROV 10-1 (5.9 ± 2.4 μg g^{-1}, $n = 12$) than in ROV 10-2 (1.1 ± 0.5 μg g^{-1}, $n = 11$) while residual U was in the same concentration range for the two cores (1.9 ± 0.2 μg g^{-1}, $n = 23$, **Figure 6**). The V distribution in the sediments was very similar for the two cores; both residual and reactive V were consistently at 118 ± 9 μg g^{-1} and 18 ± 3 μg g^{-1} ($n = 23$), respectively.

DISCUSSION

Atypical Diagenetic Sequences in the Southern OT Hydrothermal Sediments

In typical oxic hemipelagic sediments, dissolved Mn and Fe are released to subsurface pore water due to the reductive dissolution of Mn and Fe oxides during the organic matter mineralization process; Mn oxides are often reduced before Fe oxides as a

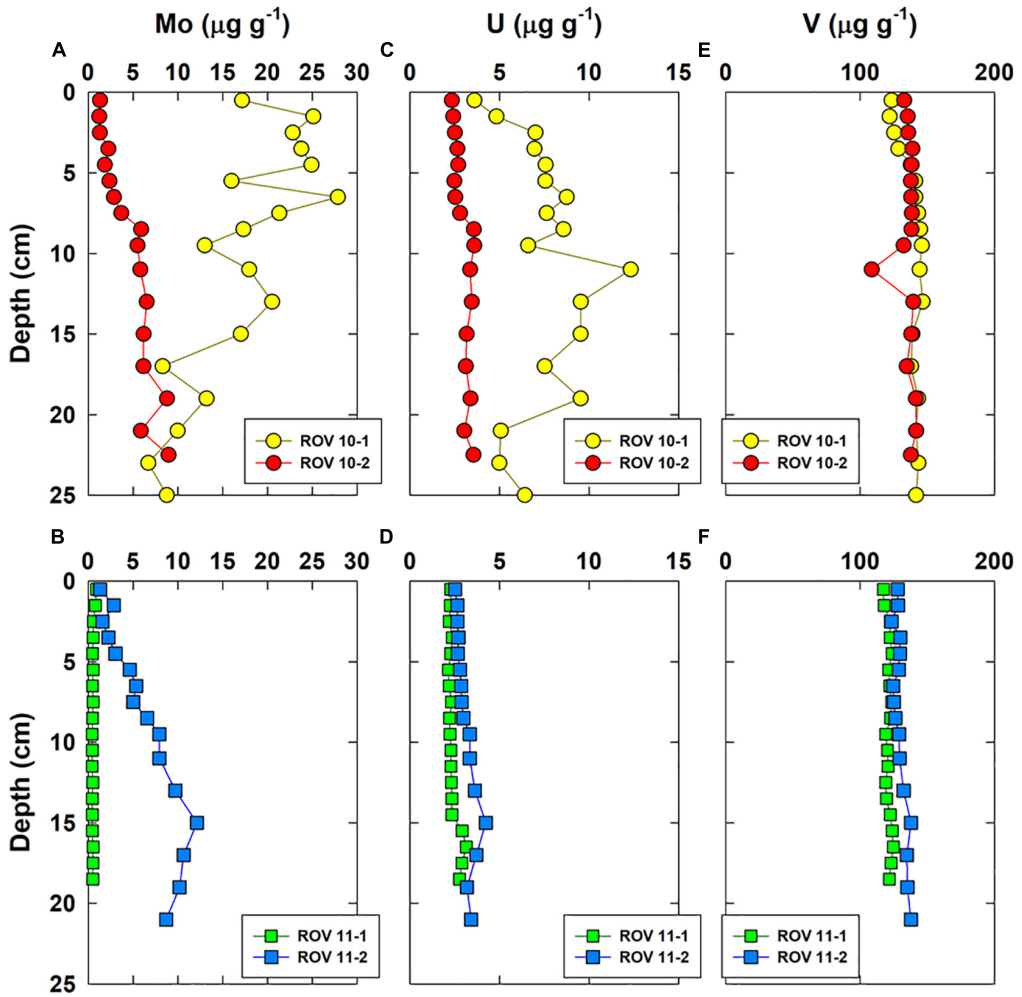

FIGURE 4 | Vertical concentration profiles of Mo **(A,B)**, U **(C,D)**, and V **(E,F)** in bulk sediments of the four cores collected from the southern Okinawa Trough.

thermodynamically favorable electron acceptor (Froelich et al., 1979). The reduction of Mn oxides often lead to a dissolved Mn peak (typically between 3 and 5 cm below the SWI; Shaw et al., 1990; Thomson et al., 1993; Dang et al., 2015; Wang et al., 2019). Dissolved Mn, during its upward transport by diffusion, could be further oxidized, resulting in an enrichment of Mn in the first few cm of the surface sediments. At stations ROV 10-2 and 11-1, we observed dissolved Mn peaks in pore water and Mn enrichments, with enrichment factors of 3.4 and 2.9, respectively (see section "Bulk Metal Concentrations in Sediment and PCA Analysis"), in surface sediments (**Figures 2C–E**, 3G,H), in agreement with the conventional literature reporting on Mn geochemistry in oxic hemipelagic sediments, as well as the sediment pore water profiles we observed in northern OT (Wang et al., 2019). However, at ROV 10-1 and ROV 11-2, Mn was not released in surface pore water (**Figures 2A–G**). Subsequently, Mn was only slightly accumulated in surface sediments (enrichment factors of 1.9 and 1.2, respectively, **Figures 3G,H**). These observations implied the absence of Mn oxide reduction in these sediments (0–10 cm of ROV10-1 and the entire core of ROV 11-2). The thermodynamically preferential Mn oxides reduction may have been inhibited by the reductive dissolution of Fe oxides, which was observed just below the SWI (**Figures 2A**, G). Dissolved, colloidal and/or particulate forms of Fe are often found to be enriched in hydrothermal plumes (Bennett et al., 2008; Tagliabue et al., 2010; Hawkes et al., 2013). Due to the observed higher fractions of Fe_{HR} in near-field hydrothermal sediments (ROV 10-1, **Figure 6**), we suggest that the unusual diagenetic sequence observed in core ROV10-1 and ROV11-2 was mainly driven by the presence of highly reactive Fe, which was used as the primary electron acceptor, instead of Mn oxides. On the other hand, other processes, such as bio-irrigation or advection (e.g., lateral transport of fluid in the sediment), could affect the diagenetic sequences, resulting in the unexpected order of redox reactions. However, because of logistic challenges (accessibility to the site), it remains challenging to assess the plausibility of these processes. Given the proximity to the hydrothermal vent (**Figure 1C**), elevated Fe concentrations (**Figure 3E**) but depletion in Al (**Figure 3A**) in the top sediments of ROV 10-1, it is more likely that the significant supply in reactive Fe would be

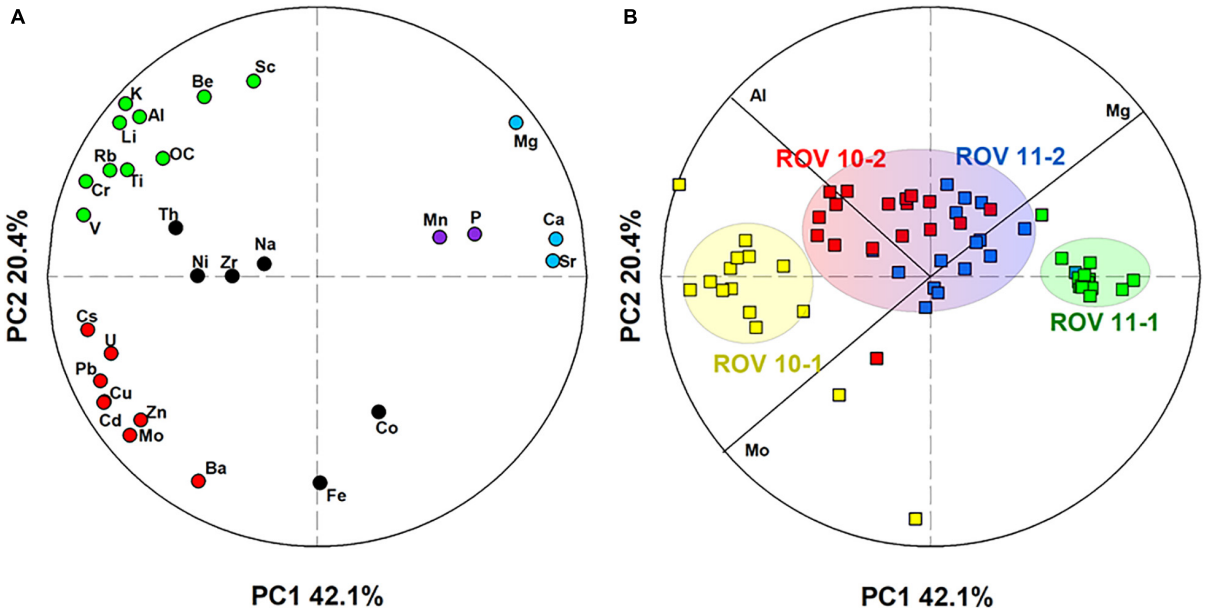

FIGURE 5 | Representation of the two principal components (PCs) obtained by PCA treatment of the dataset including **(A)** 29 elements and **(B)** 70 sediment samples. The circles represented the correlation circle. In the left panel, color codes illustrate grouping of elements by their similarities. Three groups of samples were identified in the right panel.

the dominant factor leading to the unusual diagenetic sequence observed at ROV 10-1.

In addition, below 10 cm, very low Fe_{HR} was available in the sediments, rather Fe was found in the Fe_{MAG} form which is more refractory than Fe_{OX} (see section "Metal Distribution in Sediments" and **Supplementary Figure 3**). Interestingly, both sulfide and Mn^{2+} concentrations increased in the pore water of ROV-10, just below the reactive zone of Fe where there is significantly less Fe_{HR} compared to the surface sediments (10–20 cm, **Figures 2A**, **6**). Previously, Canfield et al. (1993) have reported the co-occurrence of Fe oxides and sulfate reductions at similar depths. We suspect similar phenomenon may be happening for Mn oxides in core ROV 10-1. Moreover, elemental sulfur may also be present at ROV10-1 since it was observed in ROV10-2 (section "Vertical Profiles in Pore Water"). These factors may have combinely resulted in the co-occurrence of Mn^{2+} and HS^- in the deep sediments of ROV 10-1. Because MnS has a relatively high solubility compared to most other metals, it is possible for both Mn^{2+} and HS^- to be present in pore water at concentration levels below saturation (Smith and Martell, 1977; Huerta-Diaz et al., 1998). Iron sulfide minerals (Fe_{PY}) were also detected (up to 15% of all reactive Fe phases, **Supplementary Figure 3**). Overall, we have observed a unique diagenesis sequence in the hydrothermal-affected sediments where Fe oxides were used as the main electron acceptors in surface sediments. This observation supports the hypothesis that hydrothermal precipitates are the major source of Fe to the surrounding environment and may significantly impact diagenetic processes (Trefry and Metz, 1989).

Consequently, precipitation of Fe from the plume to the surface sediments may scavenge trace metals; we observed very high concentrations of reactive U and Mo in the sediments at station ROV 10-1. Redox-sensitive elements (Mo, U, V) are often used to indicate redox conditions at the SWI (Shaw et al., 1990; Crusius et al., 1996). In anoxic sediments, dissolved U and V in pore water are reduced to lower valences that are less soluble (Klinkhammer and Palmer, 1991; Morford et al., 2005) and the formation of thiomolybdate complexes, which are more particle-reactive, leads to Mo removal from pore water (Helz et al., 1996; Zheng et al., 2002; Vorlicek et al., 2004). As reported in section "Vertical Profiles in Pore Water", the decreasing trend in dissolved RSEs with increasing core depth was observed in all four cores. Irrespective of the extent of the authigenic RSE accumulation, their subsurface peaks were found in pore waters, i.e., ∼2 cm at ROV10-1, ∼6 cm at ROV10-2, ∼15 cm at ROV11-2. The RSE peak in ROV10-1 could be associated with the reduction of newly formed and deposited Fe oxides, as discussed above. However, at the two other stations (ROV10-2, ROV11-2), the RSE peaks followed the decline of Fe and Mn in pore water (at 5–10 cm in ROV 10-2, **Figure 2D** and at ca. 15 cm in ROV 11-2, **Figure 2H**). Because the subsurface peaks of RSEs were observed below the depth of Fe reduction but above the increase of sulide (**Figures 2C,G**), we suggest that the release of RSEs was not directly associated with the reductive dissolution of ferromanganese oxides nor the reduction of sulfate but rather a result of the formation of dissolved organic complexes. The increase in RSE concentrations in deep pore water has been reported in several sedimentary settings and was associated with dissolved organic matter that maintained RSEs in solution rather than being sequestered onto particles (Brumsack and Gieskes, 1983; Beck et al., 2008; Dang et al., 2014). The subsequent removal of RSEs (6–10 cm at ROV 10-2 or 16–25 cm at ROV 11-2) was

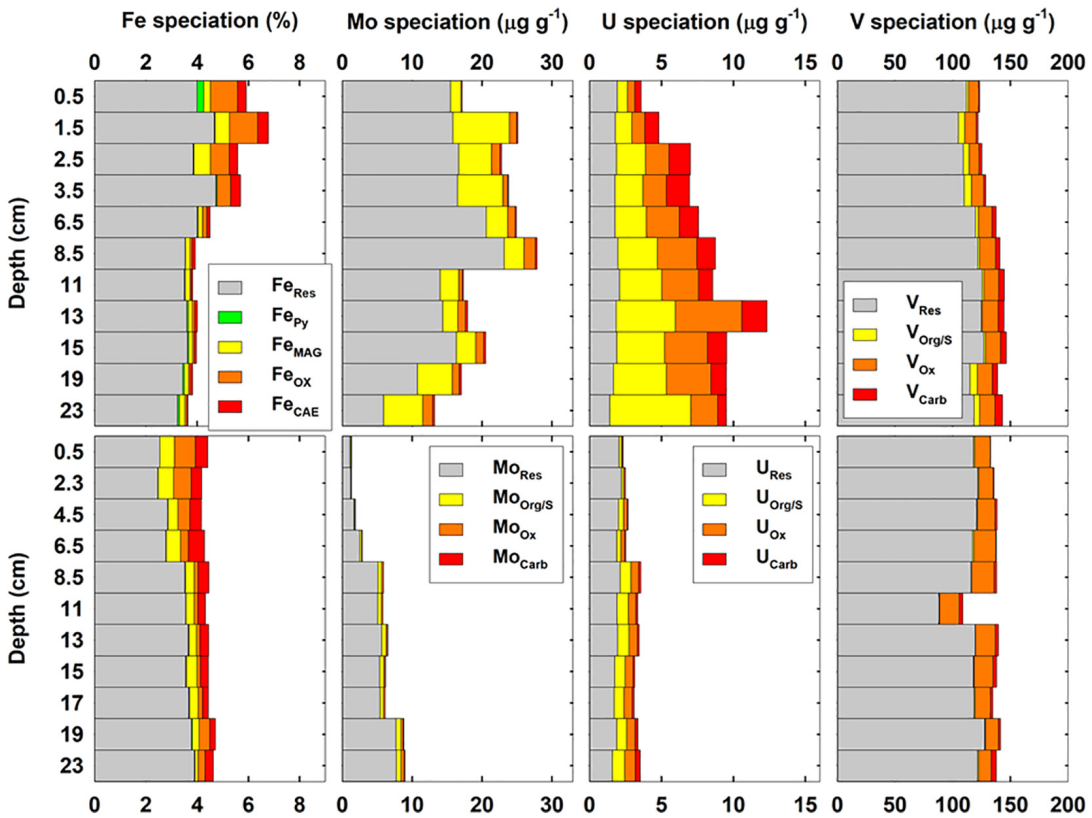

FIGURE 6 | Distribution of Fe, Mo, U, V speciation in sediments of the southern Okinawa Trough shown as absolute concentration in sediments (ROV10-1, upper panels and ROV10-2, lower panels). Highly reactive Fe (Fe_{HR}) fractions include carbonate (Fe_{CAE}), oxides (Fe_{OX}), magnetite (Fe_{Mag}), and pyrite (Fe_{Py}). Residual Fe (Fe_{Res}) is the difference between total Fe and Fe_{HR}. Similarly, labile RSEs (X = Mo, U, V) include the fractions of RSEs bound within carbonates (X_{Carb}), Fe/Mn oxides (X_{Ox}), organic/sulfides ($X_{Org/S}$). See text for further details.

concomitant with sulfide production and thus in agreement with the conventional literature (i.e., formation of particle-reactive thiomolybdate and reduction of U and V into insoluble species).

Deciphering Sources of Materials in Hydrothermal Impacted Sediments

The PCA highlighted that the lithogenic elements (i.e., group 1, section "Bulk Metal Concentrations in Sediment and PCA Analysis") were all correlated (e.g., Al, Li, Rb, **Figure 5A**). Their concentrations, as well as the elemental ratios (e.g., Ti/Al = 0.055 ± 0.002, n = 70) varied within a very narrow range in all four sediment cores ([Al] = 8.3 ± 0.4%, n = 70). The invariable sediment grain size (**Supplementary Figure 1**) and the almost constant TOC concentrations throughout the sediment cores (**Supplementary Figure 2**), indicate little change in detrital inputs in the study area.

Despite the minor variations in the lithogenic elements, there was significant variation in the carbonate-related elements (group 2, section "Bulk Metal Concentrations in Sediment and PCA Analysis") indicating processes related to carbonate mineral deposition and formation. To shed light on these mechanisms, we calculated the Mg/Ca and Sr/Ca ratios (**Figure 7A**). Similar to the outcomes of the PCA (**Figure 5B**), the four sediment cores were split into three groups. Sediments at station ROV 10-1, adjacent to the hydrothermal vent, were most depleted in carbonate minerals (i.e., highest Sr/Ca and Mg/Ca ratios), potentially due to total Mg removal and Ca cycling in the hydrothermal fluid (Antonelli et al., 2017 and references therein). These sediments, therefore, constituted one endmember of the mixing lines (**Figures 7A–C**). The other endmember is sediments from station ROV 11-1 where constant and high Mg, Ca and Sr concentrations were observed (**Figure 3D**); the low Mg/Ca and Sr/Ca ratios (**Figure 7A**) indicated that the carbonate minerals at this station were more likely to be biogenic calcite (Bayon et al., 2007).

In summary, the two endmembers reflected either the marine (ROV 11-1) or hydrothermal influences (ROV 10-1). Sediments at station ROV 10-2 and 11-2 fell on the mixing line between these two endmembers. The deep sediments were more likely to be influenced by the hydrothermal vents while the top sediments were more enriched in biogenic calcite (**Figures 3C,D**).

Hydrothermal-Impacted Geochemistry of Redox-Sensitive Elements

A negative relationship between the carbonate-related group (Mg, Ca, Sr) and trace elements (e.g., Mo, U) was observed based

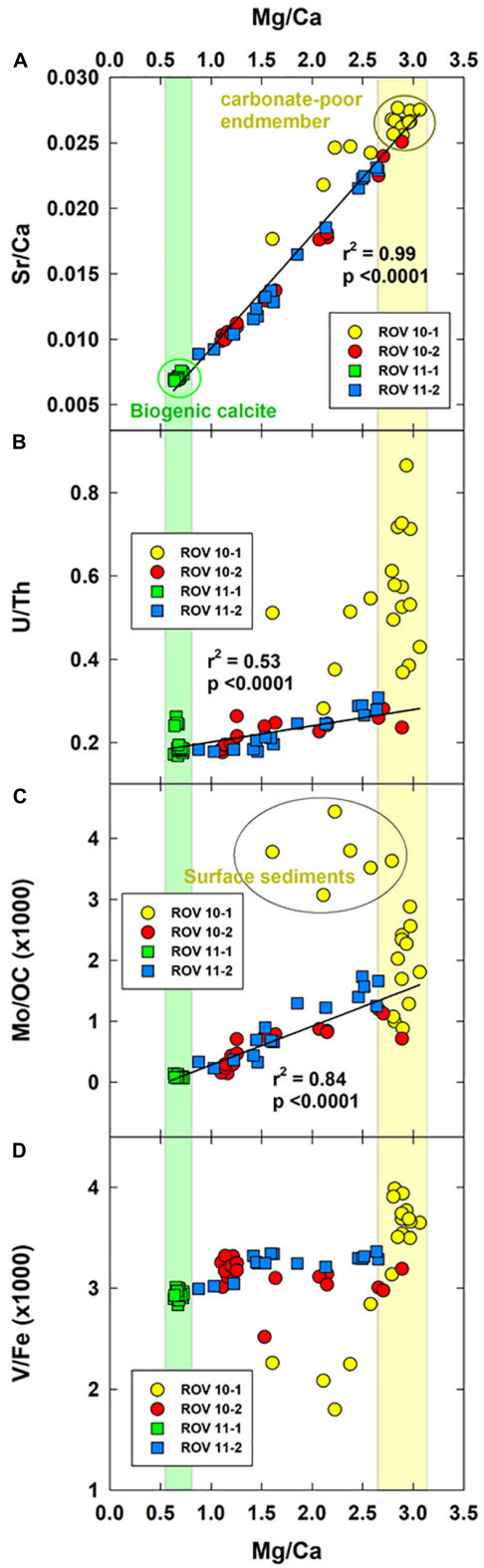

FIGURE 7 | Crossplots of Sr/Ca **(A)**, U/Th **(B)**, Mo/OC **(C)** and V/Fe **(D)** as the function of Mg/Ca. In **(A)**, the top four cm sediments at station ROV 10-1 was excluded from the regression. In **(B,C)**, the regression was performed only on ROV 10-2, 11-1, and 11-2.

on the PCA outputs (**Figure 5A**), indicating there were related geochemical processes controlling the cycle of these elements. To assess the geochemical behavior of each element, we normalized the concentrations of U, Mo and V relative to Th, OC and Fe, respectively. First, because thorium is not a redox-reactive element, the U/Th ratios indicate whether the geochemical evolution of authigenic U is related to its reductive accumulation (Cochran et al., 1986). Second, because Mo accumulation in sediments could be related either to the formation of particle-reactive thiomolybdate species or its delivery and burial with organic carbon (McManus et al., 2006 and references therein), Mo/OC ratios help decipher the difference between authigenically formed Mo and allogenic organic Mo. Finally, it has been demonstrated that hydrothermal precipitates were responsible for V removal from seawater (Feely et al., 1994; Ludford et al., 1996). Therefore, normalizing V relative to Fe, we can evaluate if hydrothermal Fe precipitates would be a major source of V deposition to the sediments.

We have shown previously (section "Bulk Metal Concentrations in Sediment and PCA Analysis") that Mo and U behaved similarly in the study area while the geochemical behavior of V approximated the lithogenic elements. Therefore, when plotted relative to the Mg/Ca ratios (**Figures 7B–D**), normalized U and Mo ratios showed a similar trend while V differed. U/Th and Mo/OC ratios were significantly correlated to that of Mg/Ca (**Figures 7B,C**), except for sediments from station ROV 10-1. This strong correlation indicated that U and Mo accumulation at these stations (ROV 10-2, 11-1, and 11-2) was mainly allogenic as it followed the mixing of the two end-members (marine and hydrothermal). As a result, the reactive Mo and U at these three stations was a minor fraction relative to the residual fraction (**Figure 6**). However, at station ROV 10-1, enrichment of U and Mo was much higher (**Figures 6**, **7B,C**) and typical of authigenic accumulation. In fact, U accumulation was more noticeable than that of Mo and is supported by the dominant reactive U fraction in ROV 10-1 sediments (**Figure 6**).

The different geochemical mechanisms leading to their authigenic accumulation could explain the discrepancy between U and Mo enrichment. First, U enrichment is directly related to the reductive accumulation of insoluble U(IV); the redox potentials of the U(IV)/U(VI) half-reaction varied between -0.046 ± 0.001 V for the half-reaction involving $Ca_2U^{VI}O_2(CO_3)_3$ and $U^{IV}O_2$ (Brooks et al., 2003). This E_h typically corresponds to the hypoxic zone of subsurface sediments where ferromanganese oxides are reduced (Couture and Van Cappellen, 2011; Alessi et al., 2014). On the other hand, Mo geochemical cycle is highly dependent on that of sulfide as Mo becomes more particle-reactive in euxinic environments because of the thiomolybdate species formation (Dang et al., 2018 and references therein). This conventional behavior is well supported by the total depletion of dissolved Mo at station ROV 10-1 and 10-2 (**Figures 2B,D**) where sulfide concentrations were detected (**Figures 2A,C**). However, we found higher authigenic U and Mo accumulation in the surface sediments of ROV 10-1 (deviation from the regression line, **Figures 7A–C**), where a high amount of reactive Mo (organic/sulfide fraction) was observed (**Figure 6**). This finding demonstrated that unique

geochemical features of this station adjacent to the hydrothermal vent (ROV 10-1, enrichment of particles of hydrothermal origins, see sections above) altered the geochemistry of Mo and U. Besides, the normalization approach we applied (U/Th and Mo/OC) here could pinpoint the authigenic and allogenic Mo and U in these sediments.

There was no clear correlation between V/Fe and Mg/Ca ratios (**Figure 7D**). However, it should be noted that V/Fe ratios did not significantly vary in all four sediment cores ($3.1 \pm 0.4 \times 10^{-3}$, $n = 70$), and reactive V represented only 15% of total V (stations ROV 10-1 and 10-2, **Figure 6**). Also, being of lithogenic origin, as shown by the results of the PCA (**Figure 5A**), V behavior was different from other trace metals.

Potential Benthic Fluxes Generated by Hydrothermal Influenced Sediments

While the hydrothermal sediments deliver a significant amount reactive Fe and other metals to the surrounding sediments, these elements are not immediately buried. Because of the atypical diagenetic sequence observed in these sediments and its subsequent impact on the geochemistry of the RSEs, it is expected that benthic fluxes in these hydrothermal sediments may differ from other pelagic sediments. Previous studies have reported shallower oxygen penetration depths and higher reactive Fe fractions in the volcanogenic sediments, which may induce higher dissolution rates of Fe and Mn oxides (Hembury et al., 2009; Homoky et al., 2011). Therefore, benthic fluxes of dissolved Fe and other metals generated by the volcanogenic/hydrothermal sediments can potentially be significant to overlying waters (Homoky et al., 2011; Aquilina et al., 2014).

Based on the fact that high dissolved Fe concentrations were measured in surficial pore water (section "Vertical Profiles in Pore Water") and also that a certain fraction (∼30–40%) of Fe_{HR} (section "Sediment Geochemistry") was quantified in the surface layer of near-field hydrothermal sediments, we calculated the fluxes of Fe and other metals that may be generated from the hydrothermal sediments. These benthic fluxes were calculated using 1-D steady-state mass conservation equations (Boudreau, 1997; supporting information **Supplementary Text 2**). Briefly, the pore water profiles served as inputs to the model and calculations (e.g., resolution of differential equations) were carried out using the computer code PROFILE (Berg et al., 1998).

The calculated benthic fluxes of Fe ranged between 16.8 and 111.1 μmol m^{-2} day^{-1} (**Table 1**) and were significantly higher than those reported in coastal California sediments (0.84 ± 0.88 μmol m^{-2}, Elrod et al., 2004), where water depths are > 1,000 m, and also along the Peruvian coast (0–1.1 μmol m^{-2} day^{-1}; Noffke et al., 2012) where water depths are between ∼700–1,000 m. The benthic flux of Fe at ROV10-1 (111 μmol m^{-2} day^{-1}) was also much higher than the Fe fluxes measured in the volcanogenic sediments in the northern Caribbean Sea (0.27–30.1 μmol m^{-2} day^{-1}; Homoky et al., 2011). However, they were comparable to the Fe fluxes found in some shallow or anoxic stations along the California coast (6–568 μmol m^{-2} day^{-1}; Severmann et al., 2010).

TABLE 1 | Calculated benthic fluxes of Fe, Mn, Mo, U, V from the sediments of the southern Okinawa Trough.

Stations	Fe	Mn	Mo	U	V
ROV10-1	111.1	5.0	81.5	−2.9	−3.5
ROV10-2	32.6	17.9	54.4	−1.7	11.1
ROV11-1	16.8	0.74	15.1	−1.9	4.7
ROV11-2	36.4	2.5	−19.4	−3.5	8.9

Units are μmol m^{-2} day^{-1} for Fe and Mn, and nmol m^{-2} day^{-1} for Mo, U, V, respectively.

On the other hand, the Mo flux calculated at ROV10-1 (81.5 nmol m^{-2} day^{-1}) was at the high end of the Mo benthic fluxes (−66.8–85.8 nmol m^{-2} day^{-1}, $n = 4$) found in Buzzards Bay, US (Morford et al., 2009). The observed Mn flux was comparable to the average dissolved Mn input from continental margins (∼11.0 μmol m^{-2} d^{-1}; Berelson et al., 2003). The U flux (1.7–3.5 nmol m^{-2} d^{-1}) was relatively comparable to those reported in coastal and shelf sediments (Barnes and Cochran, 1990; Zheng et al., 2002; McManus et al., 2005). While benthic fluxes of V are rarely reported, our calculated values were much lower than those reported in coastal areas of the northwest Iberian Peninsula (42–119 nmol m^{-2} d^{-1}; Santos-Echeandia et al., 2009).

In summary, relatively high Fe fluxes were considered significant in shallow or reducing coastal sediments. However, in deeper (>1,000 m) waters, benthic Fe fluxes were low and/or negligible. This study clearly showed that deep-sea sediments influenced by hydrothermal vents have the potential to contribute high benthic fluxes of Fe and other metals (e.g., Mo) to the overlying water column. Considering the occurrence of multiple hydrothermal fields in the middle and southern OT, metal fluxes generated from the hydrothermal sediments can be potentially important to the marine Fe budget, in addition to the hydrothermal fluids. With this said, this study only investigated a limited number of sediment cores. Although these cores were strategically important because of their proximity to hydrothermal vents, it is uncertain whether this result can be extrapolated to a bigger scale. Moving forward, more cores from a much broader region of the hydrothermal field need to be collected and studied to produce a reliable estimation of the estimated benthic fluxes of this area. Such data would greatly benefit us to better understand the geochemical cycling process of Fe and other metals in those hydrothermally influenced sediments and quantify its significance in terms of a global scale of marine trace metal budget.

CONCLUSION

We have demonstrated atypical diagnetic processes and geochemistry in the OT hydrothermal sediments and, most notably, at station ROV 10-1, which is adjacent to an active hydrothermal vent. We observed high fractions of reactive Fe, Mo and U in these hydrothermal sediments. Due to the significant high input of Fe precipitates from the vent to nearby sediments, the early diagenetic reactions involving Mn oxides in

those sediments were likely replaced by the reductive dissolution of Fe oxides just below the SWI, leading to high dissolved Fe, Mo, U concentrations below the sediment surface. Consequently, the estimated upward fluxes of these elements in the southern OT, especially adjacent to the hydrothermal vent (ROV 10-1), were much higher than those in other deep ocean sediments.

By coupling RSEs concentration ratios with carbonate mineral ratios (Sr/Ca and Mg/Ca), we have elucidated the origins of materials delivered to the study area from the end-members, i.e., hydrothermal vs. marine (hydrogenous). This approach is important because it provides a screening tool regarding the nature of sediments in an active hydrothermal seafloor in future studies. Furthermore, this approach helped identify the allogenic and authigenic origins of other trace RSEs, such as U and Mo, which uncertain detrital ratios would otherwise challenge in the allogenic fractions.

This comprehensive study on a unique set of samples collected by advanced technology provided valuable data to demonstrate distinctive early diagenesis processes in near-field hydrothermal sediments. Such study is much needed in the future to better understand the geochemical recycling process of metals at SWI in those hydrothermally influenced sediments and their potential significance to the global budget of trace metals in the marine environment.

DATA AVAILABILITY STATEMENT

All data, including sediment bulk concentrations, metal speciation, and pore water concentrations, have been uploaded to researchgate.net and can be accessed at doi: 10.13140/RG.2.2.33316.40321 or under the name "hydrothermal sediment in southern OT".

AUTHOR CONTRIBUTIONS

LL, JL, and XS designed the research. XW, YW, and AZ contributed sample collection, sample analysis, and data discussion. LL, DHD, and XW analyzed the data. LL, DHD, XW, JL, and XS wrote the manuscript. All authors contributed to the article and approved the submitted version.

FUNDING

This work was supported by the National Key Basic Research Program of China (2013CB429704), the National Natural Science Foundation of China (42076046), and the NSFC-Shandong Joint Fund for Marine Science Research Centers (U1606401).

ACKNOWLEDGMENTS

We would like to thank the captain and crew of the *R/V Ke Xue* and the pilots of the *ROV Fa Xian* for their skills and technical support at sea. We also want to thank all the colleagues and students who have helped at sea or in the laboratory to make this work possible, especially Baoju Yang, and graduate students, Xiaotong Zhen and Yijun Ren.

SUPPLEMENTARY MATERIAL

The Supplementary Material for this article can be found online at: https://www.frontiersin.org/articles/10.3389/fmars.2021.722599/full#supplementary-material

REFERENCES

Alessi, D. S., Lezama-Pacheco, J. S., Janot, N., Suvorova, E. I., Cerrato, J. M., Giammar, D. E., et al. (2014). Speciation and reactivity of uranium products formed during in situ bioremediation in a shallow alluvial aquifer. *Environ. Sci. Technol.* 48, 12842–12850. doi: 10.1021/es502701u

Antonelli, M. A., Pester, N. J., Brown, S. T., and DePaolo, D. J. (2017). Effect of paleoseawater composition on hydrothermal exchange in midocean ridges. *Proc. Natl. Acad. Sci. U.S.A.* 114, 12413–12418. doi: 10.1073/pnas.1709145114

Aquilina, A., Homoky, W. B., Hawkes, J. A., Lyons, T. W., and Mills, R. A. (2014). Hydrothermal sediments are a source of water column Fe and Mn in the Bransfield Strait, Antarctica. *Geochim. Cosmochim. Acta* 137, 64–80. doi: 10.1016/j.gca.2014.04.003

Barnes, C. E., and Cochran, J. K. (1990). Uranium removal in oceanic sediments and the oceanic U balance. *Earth Planet. Sci. Lett.* 97, 94–101. doi: 10.1016/0012-821x(90)90101-3

Bayon, G., Pierre, C., Etoubleau, J., Voisset, M., cauquil, E., Marsset, T., et al. (2007). Sr/Ca and Mg/Ca ratios in niger delta sediments: implications for authigenic carbonate genesis in cold seep environments. *Mar. Geol.* 241, 93–109. doi: 10.1016/j.margeo.2007.03.007

Beaulieu, S. E., Baker, E. T., and German, C. R. (2015). Where are the undiscovered hydrothermal vents on oceanic spreading ridges? *Deep Sea Res. II* 121, 202–212. doi: 10.1016/j.dsr2.2015.05.001

Beck, M., Dellwig, O., Schnetger, B., and Brumsack, H. J. (2008). Cycling of trace metals (Mn, Fe, Mo, U, V, Cr) in deep pore waters of intertidal flat sediments. *Geochim. Cosmochim. Acta* 72, 2822–2840. doi: 10.1016/j.gca.2008.04.013

Bennett, S. A., Achterberg, E. P., Connelly, D. P., Statham, P. J., Fones, G. R., and German, C. R. (2008). The distribution and stabilisation of dissolved Fe in deep-sea hydrothermal plumes. *Earth Planet. Sci. Lett.* 270, 157–167. doi: 10.1016/j.epsl.2008.01.048

Berelson, W., McManus, J., Coale, K., Johnson, K., Burdige, D., Kilgore, T., et al. (2003). A time series of benthic flux measurements from Monterey Bay, CA. *Cont. Shelf Res.* 23, 457–481. doi: 10.1016/s0278-4343(03)00009-8

Berg, P., Risgaard-Petersen, N., and Rysgaard, S. (1998). Interpretation of measured concentration profiles in sediment pore water. *Limnol. Oceanogr.* 43, 1500–1510. doi: 10.4319/lo.1998.43.7.1500

Boudreau, B. P. (1997). *Diagenetic Models and Their Implementation*. Berlin: Springer-Verlag.

Brooks, S. C., Fredrickson, J. K., Carroll, S. L., Kennedy, D. W., Zachara, J. M., Plymale, A. E., et al. (2003). Inhibition of bacterial U(VI) reduction by calcium. *Environ. Sci. Technol.* 37, 1850–1858. doi: 10.1021/es0210042

Brumsack, H. J., and Gieskes, J. M. (1983). Interstitial water trace-metal chemistry of laminated sediments from the Gulf of California, Mexico. *Mar. Chem.* 14, 89–106. doi: 10.1016/0304-4203(83)90072-5

Burton, E. D., Sullivan, L. A., Bush, R. T., Johnston, S. G., and Keene, A. F. (2008). A simple and inexpensive chromium-reducible sulfur method for acid-sulfate soils. *Appl. Geochem.* 23, 2759–2766. doi: 10.1016/j.apgeochem.2008.07.007

Canfield, D. E., Thamdrup, B., and Hansen, J. W. (1993). The anaerobic degradation of organic matter in Danish coastal sediments: Fe reduction, Mn reduction and sulfate reduction. *Geochim. Cosmochim. Acta* 57, 3867–3883. doi: 10.1016/0016-7037(93)90340-3

Chen, C. H., Lee, T., Shieh, Y. N., Chen, C. H., and Hsu, W. Y. (1995). Magmatism at the onset of back-arc basin spreading in the Okinawa Trough. *J. Volcanol. Geoth. Res.* 69, 313–322. doi: 10.1016/0377-0273(95)00028-3

Cline, J. D. (1969). Spectrophotometric determination of hydrogen sulfide in natural waters. *Limnol. Oceanogr.* 14, 454–458. doi: 10.4319/lo.1969.14.3.0454

Cochran, J. K., Carey, A. E., Sholkovitz, E. R., and Suprenant, L. D. (1986). The geochemistry of uranium and thorium in coastal marine sediments and sediment porewaters. *Geochim. Cosmochim. Acta* 50, 663–680. doi: 10.1016/0016-7037(86)90344-3

Couture, R.-M., and Van Cappellen, P. (2011). Reassessing the role of sulfur geochemistry on arsenic speciation in reducing environments. *J. Hazard. Mater.* 189, 647–652. doi: 10.1016/j.jhazmat.2011.02.029

Crusius, J., Calvert, S., Pedersen, T., and Sage, D. (1996). Rhenium and molybdenum enrichments in sediments as indicators of oxic, suboxic and sulfidic conditions of deposition. *Earth Planet. Sci. Lett.* 145, 65–78. doi: 10.1016/s0012-821x(96)00204-x

Dang, D. H., Evans, D. R., Wang, W., Omanovic, D., Houssainy, A. E., et al. (2018). Uranium isotope geochemistry in modern coastal sediments: insights from Toulon Bay, France. *Chem. Geol.* 481, 133–145. doi: 10.1016/j.chemgeo.2018.01.032

Dang, D. H., Lenoble, V., Durrieu, G., Omanović, D., Mullot, J. U., Mounier, S., et al. (2015). Seasonal variations of coastal sedimentary trace metals cycling: insight on the effect of manganese and iron(oxy)hydroxides, sulphide and organic matter. *Mar. Pollut. Bull.* 92, 113–124. doi: 10.1016/j.marpolbul.2014.12.048

Dang, D. H., Tessier, E., Lenoble, V., Durrieu, G., Omanović, D., Mullot, J. U., et al. (2014). Key parameters controlling arsenic dynamics in coastal sediments: an analytical and modeling approach. *Mar. Chem.* 161, 34–46. doi: 10.1016/j.marchem.2014.02.005

Dou, Y., Yang, S., Liu, Z., Clift, P. D., Yu, H., Berne, S., et al. (2010). Clay mineral evoluation in the central Okinawa Trough since 28 ka: implications for sediment provenace and paleoenvironmental change. *Palaeogeogr. Palaeoclimatol. Palaeoecol.* 288, 108–117. doi: 10.1016/j.palaeo.2010.01.040

Edmond, J. M., Measures, C., McDuff, R. E., Chan, L. H., Collier, R., Grant, B., et al. (1979). Ridge crest hydrothermal activity and the balances of the major and minor elements in the ocean–Galapagos data. *Earth Planet. Sci. Lett.* 46, 1–18. doi: 10.1016/0012-821x(79)90061-x

Elderfield, H., and Schultz, A. (1996). Mid-ocean ridge hydrothermal fluxes and chemical composition of the ocean. *Annu. Rev. Earth Planet. Sci.* 24, 191–224. doi: 10.1146/annurev.earth.24.1.191

Elrod, V. A., Berelson, W., Coale, K. H., and Johnson, K. S. (2004). The flux of iron from continental shelf sediments: a missing source for global budgets. *Geophys. Res. Lett.* 31:L12307. doi: 10.1029/2004GL020216

Feely, R. A., Massoth, G. J., Trefry, J. H., Baker, E. T., Paulson, A. J., and Lebon, G. T. (1994). Composition and sedimentation of hydrothermal plume particles from North Cleft segment, Juan de Fuca Ridge. *J. Geophys. Res. Solid Earth* 99, 4985–5006. doi: 10.1029/93jb02509

Froelich, P. N., Klinkhammer, G. P., Bender, M. L., Luedtke, N. A., Heath, G. R., Cullen, D., et al. (1979). Early oxidation of organic matter in pelagic sediments of the eastern equatorial Atlantic: suboxic diagenesis. *Geochim. Cosmochim. Acta* 43, 1075–1090. doi: 10.1016/0016-7037(79)90095-4

Gena, K., Kase, K., Chiba, H., and Nakashima, K. (2005). Tin-bearing chalcopyrite and platinum-bearing bismuthinite in the active Tiger sulfide chimney, Yonaguni Knoll IV seafloor hydrothermal system, Okinawa Trough, Japan. *EOS Trans. AGU* 86, 51C–1492C.

Glasby, G. P., and Notsu, K. (2003). Submarine hydrothermal mineralization in the Okinawa Trough, SW of Japan: an overview. *Ore Geol. Rev.* 23, 299–339. doi: 10.1016/j.oregeorev.2003.07.001

Halbach, P., Nakamura, K.-i, Wahsner, M., Lange, J., Sakai, H., Käselitz, L., et al. (1989). Probable modern analogue of Kuroko-type massive sulphide deposites in the Okinawa Trough back-arc basin. *Nature* 338, 496–499. doi: 10.1038/338496a0

Hawkes, J. A., Connelly, D. P., Gledhill, M., and Achterberg, E. P. (2013). The stabilisation and transportation of dissolved iron from high temperature hydrothermal vent systems. *Earth Planet. Sci. Lett.* 375, 280–290. doi: 10.1016/j.epsl.2013.05.047

Hawkes, J. A., Connelly, D. P., Rijkenberg, M. J. A., and Achterberg, E. P. (2014). The importance of shallow hydrothermal island arc systems in ocean biogeochemistry. *Geophys. Res. Lett.* 41, 942–947. doi: 10.1002/2013GL058817

Helz, C. R., Miller, C. V., Charnock, J. M., Mosselmans, J. F. W., Pattrick, R. A. D., Garner, C. D., et al. (1996). Mechanism of molybdenum removal from the sea and its concentration in black shales: EXAF evidence. *Geochim. Cosmochim. Acta* 60, 3631–3642. doi: 10.1016/0016-7037(96)00195-0

Hembury, D., Palmer, M. R., Fones, G. R., and Jones, M. T. (2009). Oxygen uptake during marine diagenesis of fresh volcanic material. *Geochim. Cosmochim. Acta* 73:A521.

Homoky, W. B., Hembury, D. J., Hepburn, L. E., Mills, R. A., Statham, P. J., Fones, G. R., et al. (2011). Iron and manganese diagenesis in deep sea volcanogenic sediments and the origins of pore water colloids. *Geochim. Cosmochim. Acta* 75, 5032–5048. doi: 10.1016/j.gca.2011.06.019

Honda, M. C., Kusakabe, M., Nakabayashi, S., and Katagiri, M. (2000). Radiocarbon of sediment trap samples from the Okinawa trough: lateral transport of ^{14}C-poor sediment from the continental slope. *Mar. Chem.* 68, 231–247. doi: 10.1016/s0304-4203(99)00080-8

Huerta-Diaz, M. A., Tessier, A., and Carignan, R. (1998). Geochemistry of trace metals associated with reduced sulfur in freshwater sediments. *Appl. Geochem.* 13, 213–233. doi: 10.1016/s0883-2927(97)00060-7

Inagaki, F., Kuypers, M. M., Tsunogai, U., Ishibashi, J., Nakamura, K., Treude, T., et al. (2006). Microbial community in a sediment-hosted CO_2 lake of the southern Okinawa Trough hydrothermal system. *Proc. Natl. Acad. Sci. U.S.A.* 103, 14164–14169. doi: 10.1073/pnas.0606083103

Kao, S. J., Wu, C. R., Hsin, Y. C., and Dai, M. H. (2006). Effects of sea level change on the upstream Kuroshio Current through the Okinawa Trough. *Geophys. Res. Lett.* 33:L16604.

Kawagucci, S., Chiba, H., Ishibashi, J.-I., Yamanaka, T., Toki, T., Muramatsu, Y., et al. (2011). Hydrothermal fluid geochemistry at the Iheya North field in the mid-Okinawa Trough: implication for origin of methane in subseafloor fluid circulation systems. *Geochem. J.* 45, 109–124. doi: 10.2343/geochemj.1.0105

Kinoshita, M., Yamano, M., Post, J., and Halbach, P. (1990). Heat flow measurements in the central and southern Okinawa Trough on R/V Sonne in 1998. *Bull. Earthq. Res. Inst.* 65, 571–588.

Klinkhammer, G. P., and Palmer, M. R. (1991). Uranium in the oceans: where it goes and why. *Geochim. Cosmochim. Acta* 55, 1799–1806. doi: 10.1016/0016-7037(91)90024-y

Konno, U., Tsunogai, U., Nakagawa, F., Nakaseama, M., Ishibashi, J., Nunoura, T., et al. (2006). Liquid CO2 venting on the seafloor: Yonaguni knoll VI hydrothermal system, Okinawa Trough. *Geophys. Res. Lett.* 33:L16607.

Kuo, F. W., and Chen, C. T. (2000). Preliminary investigation of shallow hydrothermal vents off northeastern Taiwan. *EOS Trans. AGU* 81:W86.

Li, L., Liu, J. H., Wang, X. J., and Shi, X. F. (2015). Dissolved trace metal distributions and Cu speciation in the southern Bohai Sea, China. *Mar. Chem.* 172, 34–45. doi: 10.1016/j.marchem.2015.03.002

Ludford, E. M., Palmer, M. R., German, C. R., and Klinkhammer, G. P. (1996). The geochemistry of Atlantic hydrothermal particles. *Geophys. Res. Lett.* 23, 3503–3506. doi: 10.1029/96gl02078

Machiyama, H., Shinjo, R., Hattori, M., Okano, M., Matsumoto, T., Kimura, M., et al. (2001). Outline of dolphin-3 K dive surveys on the Kuroshima Knoll and in the southern Okinawa Trough-preliminary report of the NT00-05 Cruise. *JAMSTECTR Deep Sea Res.* 18, 15–30.

Matsuno, T., Lee, J.-S., and Yanao, S. (2009). The Kuroshio exchange with the South and East China Seas. *Ocean Sci.* 5, 303–312. doi: 10.5194/os-5-303-2009

McManus, J., Berelson, W. M., Klinkhammer, G. P., Hammond, D. E., and Holm, C. (2005). Authigenic uranium: relationship to oxygen penetration depth and organic carbon rain. *Geochim. Cosmochim. Acta* 69, 95–108. doi: 10.1016/j.gca.2004.06.023

McManus, J., Berelson, W. M., Severmann, S., Poulson, R. L., Hammond, D. E., Klinkhammer, G. P., et al. (2006). Molybdenum and uranium geochemistry in continental margin sediments: paleoproxy potential. *Geochim. Cosmochim. Acta* 70, 4643–4662. doi: 10.1016/j.gca.2006.06.1564

Morford, J. L., and Emerson, S. (1999). The geochemistry of redox sensitive trace metals in sediments. *Geochim. Cosmochim. Acta* 63, 1735–1750.

Morford, J. L., Emerson, S. R., Breckel, E., and Kim, S. H. (2005). Diagenesis of oxyanion (V, U, Re and Mo) in pore water and sediments from a continental margin. *Geochim. Cosmochim. Acta* 69, 5021–5032. doi: 10.1016/j.gca.2005.05.015

Morford, J. L., Martin, W. R., François, R., and Carney, C. M. (2009). A model for uranium, rhenium, and molybdenum diagenesis in marine sediments based on results from coastal locations. *Geochim. Cosmochim. Acta* 73, 2938–2960. doi: 10.1016/j.gca.2009.02.029

Narita, H., Harada, K., and Tsunogai, S. (1990). Lateral transport of sediment in particles in the Okinawa Trough determined by natural radionuclides. *Geochem. J.* 24, 207–216. doi: 10.2343/geochemj.24.207

Noffke, A., Hensen, C., Sommer, S., Scholz, F., Bohlen, L., Mosch, T., et al. (2012). Benthic iron and phosphorus fluxes across the Peruvian oxygen minimum zone. *Limnol. Oceanogr.* 3, 851–867. doi: 10.4319/lo.2012.57.3.0851

Poulton, S. W., and Canfield, D. E. (2005). Development of a sequential extraction procedure for iron: implications for iron partitioning in continentally derived particulates. *Chem. Geol.* 214, 209–221. doi: 10.1016/j.chemgeo.2004.09.003

Raiswell, R., and Canfield, D. E. (2012). The iron biogeochemical cycle past and present. *Geochem. Perspect.* 1, 1–220. doi: 10.7185/geochempersp.1.1

Rauret, G., Lopezsanchez, J. F., Sahuquillo, A., Rubio, R., Davison, C., Ure, A., et al. (1999). Improvement of the BCR three step sequential extraction procedure prior to the certification of new sediment and soil reference materials. *J. Environ. Monit.* 1, 57–61. doi: 10.1039/a807854h

Santos-Echeandia, J., Prego, R., Cobelo-Garcia, A., and Millward, G. E. (2009). Porewaer geochemistry in a Galician Ria (NW Iberian Peninsula): implications for benthic fluxes of dissolved trace elements (Co, Bu, Ni, Pb, V, Zn). *Mar. Chem.* 117, 77–87. doi: 10.1016/j.marchem.2009.05.001

Severmann, S., McManus, J., Berelson, W. M., and Hammond, D. E. (2010). The continental shelf benthic iron flux and its isotope composition. *Geochim. Cosmochim. Acta* 74, 3984–4004. doi: 10.1016/j.gca.2010.04.022

Shaw, T. J., Gieskes, J. M., and Jahnke, R. A. (1990). Early diagenesis in differing depositional environments: the response of transition metals in pore water. *Geochim. Cosmochim. Acta* 54, 1233–1246. doi: 10.1016/0016-7037(90)90149-f

Sibuet, J. C., Letouzey, J., Barbier, F., Charvet, J., Foucher, J. P., Hilde, T. W. C., et al. (1987). Back arc extension in the Okinawa Trough. *J. Geophys. Res.* 92, 14041–14063.

Smith, R. M., and Martell, A. E. (1977). *Critical Stability Constants*. New York, NY: Plenum Press.

Suzuki, R., Ishibashi, J. I., Nakaseama, M., Konno, U., Tsunogai, U., Gena, K., et al. (2008). Diverse range of mineralization induced by phase separation of hydrothermal fluid: case study of the Yonaguni Knoll IV hydrothermal field in the Okinawa Trough back-arc basin. *Resour. Geol.* 58, 267–288. doi: 10.1111/j.1751-3928.2008.00061.x

Tagliabue, A., Bopp, L., Dutay, J.-C., Bowie, A. R., Chever, F., Jean-Baptiste, P., et al. (2010). Hydrothermal contribution to the oceanic dissolved iron inventory. *Nat. Geosci.* 3, 252–256. doi: 10.1038/ngeo818

Thomson, J., Higgs, N. C. I., Croudace, W., Colley, S., and Hydes, D. J. (1993). Redox zonation of elements at an oxic/post-oxic boundary in deep-sea sediments. *Geochim. Cosmochim. Acta* 57, 579–595. doi: 10.1016/0016-7037(93)90369-8

Trefry, J. H., and Metz, S. (1989). Role of hydrothermal precipitates in the geochemical cycling of vanadium. *Nature* 342, 531–533. doi: 10.1038/342531a0

Tsuji, T., Takai, K., Oiwane, H., Nakamura, Y., Masaki, Y., Kumagaib, M., et al. (2012). Hydrothermal fluid flow system around the Iheya Knoll in the mid-Okinawa Trough based on seismic reflection data. *J. Volcanol. Geothermal Res.* 213, 41–50. doi: 10.1016/j.jvolgeores.2011.11.007

Vorlicek, T. P., Kahn, M. D., Kasuya, Y., and Helz, G. R. (2004). Capture of molybdenum in pyrite forming sediments: role of ligand-induced reduction by polysulfides. *Geochim. Cosmochim. Acta* 68, 547–556. doi: 10.1016/s0016-7037(03)00444-7

Wang, X. J., Li, L., Liu, J. H., Wu, Y. H., Gao, J. J., Cao, P., et al. (2019). Early diagenesis of redox-sensitive trace metals in the northern Okinawa Trough. *Acta Oceanol. Sinica* 38, 14–25. doi: 10.1007/s13131-019-1512-5

Watanabe, M., Hoshino, K., Shiokawa, R., Takaoka, Y., Fukumoto, H., Shibata, Y., et al. (2006). Metallic mineralization associated with pillow basalts in the Yaeyama Central Graben, South Okinawa Trough, Japan. *JAMSTECTR Deep Sea Res.* 3, 1–8. doi: 10.5918/jamstecr.3.1

Yamano, M., Uyeda, S., Foucher, J. P., and Sibuet, J. C. (1989). Heat flow anomaly in the Middle Okinawa Trough. *Tectonophysics* 159, 307–318. doi: 10.1016/0040-1951(89)90136-4

Zhai, S. K., Xu, S. M., Yu, Z. H., Qin, Y. S., and Zhao, Y. Y. (2001). Two possible hydrothermal vents in the northern Okinawa Trough. *Chin. Sci. Bull.* 46, 943–945. doi: 10.1007/bf02900472

Zheng, Y., Anderson, R. F., van Geen, A., and Fleisher, M. Q. (2002). Remobilization of authigenic uranium in marine sediments by bioturbation. *Geochim. Cosmochim. Acta* 66, 1759–1772. doi: 10.1016/s0016-7037(01)00886-9

Conflict of Interest: The authors declare that the research was conducted in the absence of any commercial or financial relationships that could be construed as a potential conflict of interest.

Publisher's Note: All claims expressed in this article are solely those of the authors and do not necessarily represent those of their affiliated organizations, or those of the publisher, the editors and the reviewers. Any product that may be evaluated in this article, or claim that may be made by its manufacturer, is not guaranteed or endorsed by the publisher.